

Production of 0.5-TW Proton Pulses with a Spherical Focusing, Magnetically Insulated Diode

D. J. Johnson, G. W. Kuswa, A. V. Farnsworth, Jr., J. P. Quintenz, R. J. Leeper, E. J. T. Burns, and S. Humphries, Jr.

Sandia Laboratories, Inc., Albuquerque, New Mexico 87115

(Received 24 October 1978)

The production, focusing, and numerical simulation of a 0.5-TW proton beam is reported. This beam is produced with a spherical, magnetically insulated, ion diode fed symmetrically by the dual-pulse-line Proto I generator. The ions are accelerated with electric fields due to a virtual cathode supported by magnetic field surfaces. Approximately 75% of the diode electrical power is delivered to ions and 25% of the ion beam is focused upon thin, 1-cm-diam, 1-cm-long conical targets to produce the first experimental ion-driven implosions.

Recent advances have been made in sources of intense pulsed ion beams for magnetic and inertial confinement fusion.¹⁻³ The reduction of electron loss is accomplished via the self magnetic field in a pinched electron-beam diode,¹ the reflexing of electrons in a reflex triode,² and an applied magnetic field in a magnetically insulated (MI) diode.³ We report the production of a converging proton beam with a MI diode driven by the 10¹²-W Proto I dual-pulse-line generator.⁴ A proton beam with peak current of 360 kA at voltages between 0.8 and 1.4 MV has been diagnosed and focused with 25% efficiency onto thin conical targets with nominal lengths and diameters of 1 cm.

The apparatus is shown in Fig. 1. The applied magnetic field rises in 70 μ sec and is spherically contoured in the diode gap by the 15-cm radius aluminum anode. The anode then is pulsed positive via the center electrode of the disk triplate transmission line of the Proto I generator. A virtual cathode then is produced by electrons which are emitted from the cathode disks and spiral axially along magnetic field lines to establish a uniform equipotential surface near the anode. Anode plasma from a nylon mesh mounted upon the anode (thought to be formed by surface flashover or leakage electrons) is the source of protons or higher-*Z* ions which are accelerated. Since all magnetic field lines are contained between the anode surface (neglecting a 2-mm magnetic field soak in) and diode center line, the ions are emitted from the anode with zero canonical angular momentum and ideally can be focused to the center line. When drifting through the magnetic field, the ions are space-charge neutralized by electrons emitted from the walls of the drift region.

The diode was numerically simulated with a two-dimensional (2D) steady-state, particle-in-cell code⁵ with electron and ion motion treated

in self-consistent electric and magnetic fields. The applied and self magnetic fields, which are excluded from the anode but fully penetrate the thin disk cathodes, are computed by solving the one-component vector-potential equation. Figure 2 contains a typical instantaneous ion simulation-particle map together with lines of equal intensity B_{app} assuming cylindrical symmetry for the diode. The assumed diode voltage is 1.2 MV and B_{app} in the diode gap is 13 kG. A typical electron trajectory is shown at the position of the virtual cathode near one B_{app} field line. Complete space-charge neutralization was assumed between the disks in this simulation and hence the only electric field which exists there is the small amount which penetrates the virtual cathode. The mag-

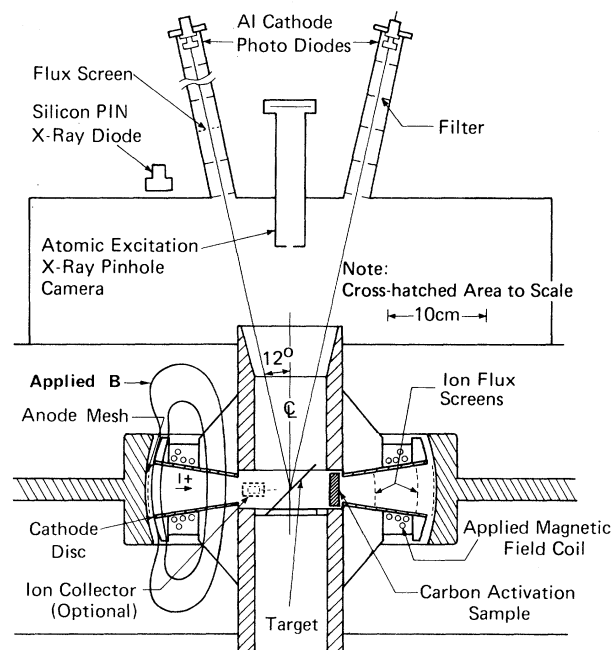


FIG. 1. Schematic of the apparatus.

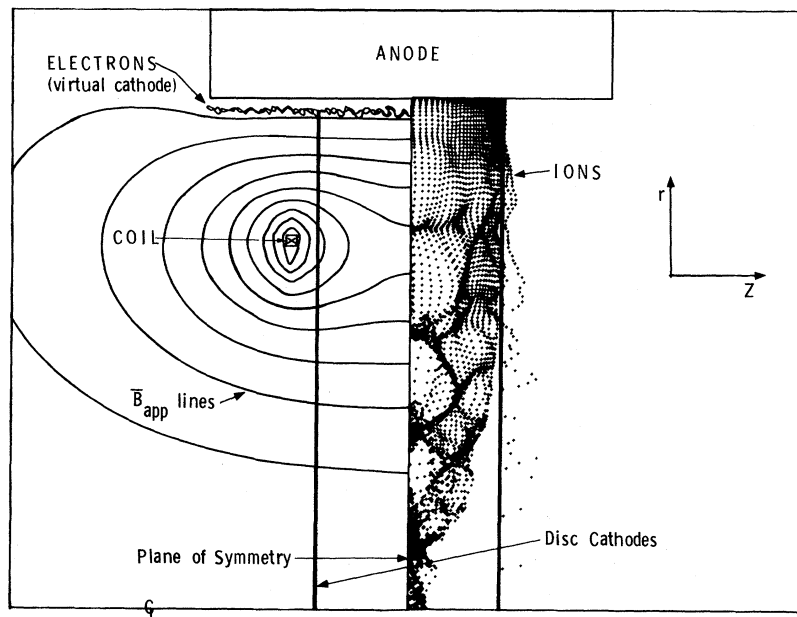


FIG. 2. Results from the numerical simulation of the diode operation. Applied magnetic-field lines and a typical electron orbit are shown to the left of the plane of symmetry, whereas an ion particle map is shown to the right.

netic field component in this region due to the ion return current on axis causes the laminar self-pinch ion flow shown by the ion map in Fig. 2. When the space-charge electric field between the disks was not set equal to zero in an attempt to simulate the neutralization process numerically, large fluctuating potential wells developed between the disks and only 10% of the beam was transported to the diode center line. This must be compared to a 90% transport efficiency for the simulation with complete space-charge neutralization. There is experimental evidence that these space-charge-produced potential wells are much weaker than calculated, possibly because of time-dependent effects not included in the code. The simulation of Fig. 2 predicts a total proton current of 270 kA and an electron current of 100 kA. This ion current is approximately 3 times larger than the value predicted by the Langmuir-Blodgett model⁶ because of electrons trapped in the diode by B_{app} .

Typical electrical characteristics of the diode are shown in the inset of Fig. 3. These data were taken with a diode gap of 8 mm, an anode ion-emitting area of 414 cm², and B_{app} of 13.5 kG ($nI = 160$ kA for each coil) in the diode gap. The electron current was determined by monitoring the total thick-target bremsstrahlung from the diode on a time-resolved basis using a silicon $p-i-n$ diode. With no nylon mesh (nearly zero ion

current) the total diode current was only 50 kA at a diode voltage of 2 MV. The thick-target electron-beam bremsstrahlung was assumed to scale with $V^{1.5}$ on the basis of the x-ray conversion efficiency⁷ for an aluminum target at an observation angle of 90°. These measurements placed an upper limit to the peak electron current of 100–125 kA for the ion-beam experiments.

The total proton current was measured using the carbon activation technique⁸ whereby the delayed positron emission from N^{13} from the reactions $C^{12}(p, \gamma)N^{13}$ and $C^{12}(d, n)N^{13}$ is observed. During data reduction an allowance was made from the yield due to the natural abundance of deuterium on the basis of the simultaneous diode current and voltage. At the 5-cm radius one or two 34%-transmission stainless-steel flux screens were used to attenuate the ion beam and a peak ion-current density of 3.5 kA/cm² was measured. At a radius of 13.5 cm, just behind the virtual cathode surface, the peak ion-current density was observed to be 1 kA/cm². These currents were in agreement with ion-collector⁹ signals observed at equal radii. The ion-collector signals also compared favorably with a calculated ion current allowing for proton time of flight by numerically time-dispersing the diode current for the ion velocity attributed to the associated instantaneous diode voltage. These diagnostics indicate peak ion currents of approximately 360

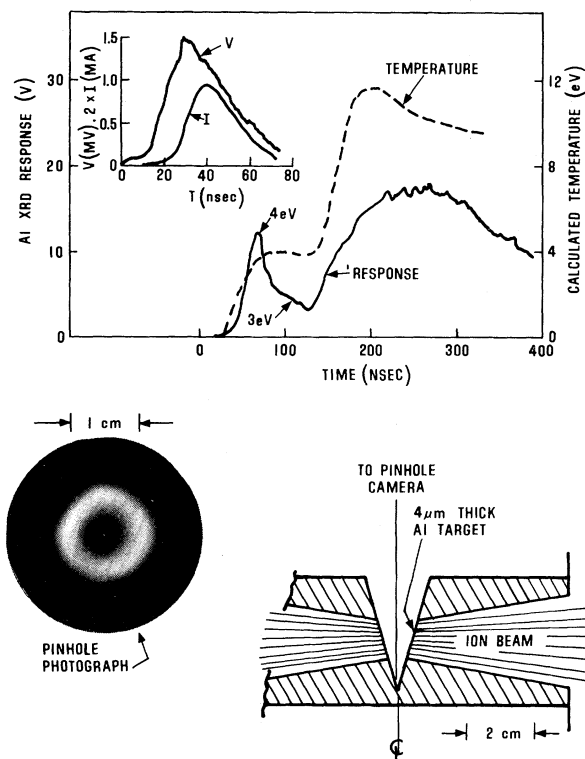


FIG. 3. A schematic of the thin conical target assembly showing the uniformity of proton-beam irradiation. The signal from a photodiode (x-ray diode) responding to the thermal radiation from the target is shown with the foil midplane temperature calculated as a function of time with LASNEX. Also shown are the corrected diode voltage (V) and total diode current (I).

and 230 kA at the 13.5- and 5-cm radii, respectively. Approximately 20% of the initial ion current would be lost between these radii upon eight coil support ribs because of the "S"-shaped orbits which protons follow when passing through B_{app} .

The focused proton-beam profile was determined for planar targets oriented at 45° to the diode center line, as shown in Fig. 1, with a pinhole camera which observed the 1.49-keV aluminum K -line radiation produced by proton-induced atomic excitation.¹⁰ Densitometer scans of the beam profile recorded in photographs obtained with 4- μ m-thick aluminum targets indicate that 10% of the 230-kA ion current entering the diode hub lies within a radius of 0.28 mm from the diode center whereas 50% lies within a radius of 0.95 mm from the center.

The temperature of these foils was estimated via analysis of line-emission spectra and by comparing the absolute magnitude of the aluminum-

cathode photodiode signals with calculated values for a blackbody source versus temperature. An extreme-uv grazing-incidence spectrograph¹¹ (88° angle of incidence, 1200 lines per mm grating) viewed the time-integrated spectrum between 60 and 600 eV. The dominant line emission associated with aluminum atoms were the $3d-2p$ electron transitions for Al VIII (Al^{7+}), Al VII, and Al VI. Oxygen line emission primarily from the $3p-2s$ transitions of OVI and OV were also observed and an upper bound for an electron density of 10^{20} cm^{-3} was obtained by attributing the observed linewidths to Stark broadening. Then, if we assume electron densities of 10^{18} - 10^{20} cm^{-3} , the observed line intensity ratios of 0.5 and 0.2 for oxygen imply a local electron temperature of $15 \pm 2 \text{ eV}$. This must be compared to a 10-eV blackbody-radiation temperature determined from the photodiodes. These observations are consistent with a LASNEX¹² Lagrangian hydrodynamic calculation for the target assuming an ion-current density of 40 kA/cm^2 (60° slant angle) and 15% of the current in the form of carbon. Because of the much shorter carbon range, an optically thin outer layer of the expanding foil was heated to approximately 15 eV in the calculation, while the bulk of the foil attained a 10-eV temperature from the proton current alone.

Data were also obtained with thin conical targets, as shown in Fig. 3, which allowed symmetrical target irradiation and current return. The cone was fabricated from 4- μ m-thick aluminum with 15° half-angle, 1.24 cm length, and 0.9-cm center-plane diameter. A peak current density of 25 kA/cm^2 was estimated for the cone from the absolute density of the exposed film from the atomic excitation pinhole camera. This result was obtained using numerically calculated¹³ x-ray-production efficiencies for the voltage and relative current through the pulse, the foil geometry used, and the sensitivity¹⁴ of the Kodak No-Sceen x-ray film used. A comparison value of 20 kA/cm^2 was obtained using 1-cm-diam carbon activation targets with three to five 34%-transmission flux screens.

A numerical simulation of the conical target response to the 25-kA/cm^2 beam was performed using LASNEX. Plotted in Fig. 3 with the photodiode (x-ray diode) response is the calculated temperature at the midplane of the foil inner surface. The initial temperature rise and photodiode signal result from the direct ion-beam deposition. At the end of the ion pulse the temperature drops somewhat and the nonobscured visible

area is reduced by the foil implosion. The second, larger temperature rise occurs as the foil self-collides at the axis of symmetry producing the high-temperature but low-area radiation signal observed by the photodiode.

It has been shown that a high-intensity ion beam can be extracted from a magnetically insulated ion diode and focused at the diode center line. The observed 75% ion production efficiency agrees with the numerical simulation value although a 37% smaller diode gap was used in the simulation. This is at least partially attributed to a 1-mm reduction in the experimental gap due to gap closure (5 cm/ μ sec was required to explain the observed time-dependent impedance) and also a 2-mm reduction in gap due to the anode plasma thickness. The observed beam profile specifies a half-angle divergence of 3.5° which must be attributed to a combination of anode emittance, space-charge blowup, and self-magnetic-field bending. In the simulation with perfect neutralization, 90% of the beam arrived at the diode center line whereas only 10% arrived in the attempt to simulate the neutralization process numerically. This must be compared to 25% (ignoring geometric considerations) in the experiment, suggesting that the actual neutralization is between the two simulations.

The authors wish to thank D. Wenger for invaluable experimental assistance, J. R. Hadley for numerous magnetic-field calculations, and J. W. Poukey and Shyke A. Goldstein for several

useful discussions concerning this work.

¹Shyke A. Goldstein, G. Cooperstein, Roswell Lee, D. Mosher, and S. J. Stephanakis, *Phys. Rev. Lett.* **40**, 1504 (1978).

²J. Golden, C. A. Kapetanakis, S. J. Marsh, and S. J. Marsh, and S. J. Stephanakis, *Phys. Rev. Lett.* **38**, 130 (1977).

³S. Humphries, Jr., R. N. Sudan, and L. Wiley, *J. Appl. Phys.* **47**, 2382 (1976).

⁴K. R. Prestwich, *IEEE Trans. Nucl. Sci.* **22**, 975 (1975).

⁵J. P. Quintenz, *J. Appl. Phys.* **49**, 4377 (1978).

⁶I. Langmuir and K. B. Blodgett, *Phys. Rev.* **22**, 347 (1923).

⁷H. W. Koch and J. W. Motz, *Rev. Mod. Phys.* **31**, 920 (1959).

⁸F. C. Young, J. Golden, and C. A. Kapetanakis, *Rev. Sci. Instrum.* **48**, 432 (1977).

⁹C. Eichenberger, S. Humphries, Jr., J. Maenchen, and R. N. Sudan, *J. Appl. Phys.* **48**, 1449 (1977).

¹⁰H. Tawara, Y. Hachiya, K. Ishii, and S. Morita, *Phys. Rev. A* **13**, 13 (1976).

¹¹D. L. Garrett and R. Tousey, *Appl. Opt.* **16**, 898 (1977). (We obtained this spectrograph on loan from G. A. Doschek and U. Feldman, Naval Research Laboratory, Washington, D. C.)

¹²G. B. Zimmerman and W. L. Kruer, *Comments Plasma Phys.* **2**, 51 (1975).

¹³D. Mosher, private communication.

¹⁴C. M. Dozier, D. B. Brown, L. S. Birks, P. B. Lyons, and R. F. Benjamin, *J. Appl. Phys.* **47**, 3732 (1976).

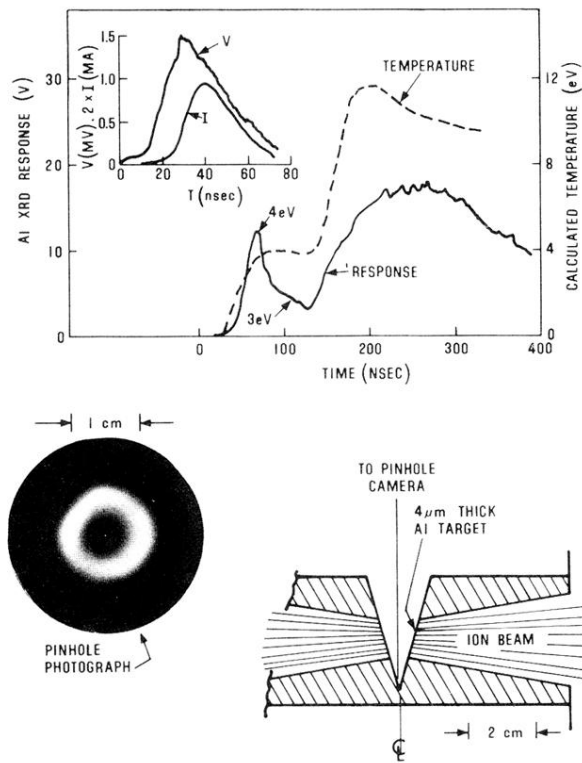


FIG. 3. A schematic of the thin conical target assembly showing the uniformity of proton-beam irradiation. The signal from a photodiode (x-ray diode) responding to the thermal radiation from the target is shown with the foil midplane temperature calculated as a function of time with LASNEX. Also shown are the corrected diode voltage (V) and total diode current (I).